Interactions between N- and C-Terminal Domains of the *Saccharomyces cerevisiae* High-Mobility Group Protein HMO1 Are Required for DNA Bending†

Kevin T. Bauerle,‡,§ Edwin Kamau,§,|| and Anne Grove*

Department of Biological Sciences, Louisiana State University, Baton Rouge, Louisiana 70803

Received November 7, 2005; Revised Manuscript Received January 9, 2006

ABSTRACT: The *Saccharomyces cerevisiae* high-mobility group protein HMO1 is composed of two DNA-binding domains termed box A and box B, of which only box B is predicted to adopt a HMG fold, and a lysine-rich C-terminal extension. To assess the interaction between individual domains and their contribution to DNA binding, several HMO1 variants were analyzed. Using circular dichroism spectroscopy, thermal stability was measured. While the melting temperatures of HMO1-boxA and HMO1-boxB are 57.2 and 47.2 °C, respectively, HMO1-boxBC, containing box B and the entire C-terminal tail, melts at 46.1 °C, suggesting little interaction between box B and the tail. In contrast, full-length HMO1 exhibits a single melting transition at 47.9 °C, indicating that interaction between box A and either box B or the tail destabilizes this domain. As HMO1-boxAB, lacking only the lysine-rich C-terminal segment, exhibits two melting transitions at 46.0 and 63.3 °C, we conclude that the destabilization of the box A domain seen in full-length HMO1 is due primarily to its interaction with the lysine-rich tail. Determination of DNA substrate specificity using electrophoretic mobility shift assays shows unexpectedly that the lysine-rich tail does not increase DNA binding affinity but instead is required for DNA bending by full-length HMO1; HMO1-boxBC, lacking the box A domain, also fails to bend DNA. In contrast, both HMO1 and HMO1-boxAB, but not the individual HMG domains, exhibit preferred binding to constrained DNA minicircles. Taken together, our data suggest that interactions between box A and the C-terminal tail induce a conformation that is required for DNA bending.

High-mobility group (HMG)[1] proteins are relatively abundant non-histone nuclear proteins with one or more homologous HMG-box DNA binding domains (*1*, *2*). The HMG box is ∼80 amino acids long and adopts an L-shaped fold composed of three α-helices (*3*−*9*). DNA binding occurs from the minor groove through partial intercalation of one or two conserved hydrophobic residues, resulting in a sharp DNA bend and helical underwinding. HMGB proteins also bind preferentially to distorted DNA such as four-way junctions, constrained minicircles, or DNA modified by the anticancer agent cisplatin [*cis*-diamminedichloroplatinum-(II)] (*6*, *10*, *11*).

Members of the protein family are subdivided according to their function and specificity of DNA binding, with moderately sequence-specific members including transcription factors such as sex-determining factor SRY and lymphoid enhancer factor LEF-1, while the non-sequence-specific family is represented by architectural chromatin-associated factors HMGB1 and -2. HMGB1 and -2 proteins have been implicated in numerous DNA-dependent activities, including DNA replication, repair, recombination, and transcription due to their ability to promote formation of higher-order nucleoprotein complexes (*1*, *2*).

Vertebrate HMGB1 contains two HMG domains, termed box A and box B, followed by an acidic C-terminal extension which modulates DNA recognition. While the acidic tail lowers the DNA binding affinity for most DNA substrates, it appears to have little effect on binding to DNA minicircles (*12*, *13*). It was not established whether this is a consequence of interaction of the tail with the HMG box(es) or the basic N-terminal extension, or if it is simply charge repulsion; however, the interaction of the C-terminal tail with one of the HMG boxes, and the absence of interaction between HMG domains, have been reported (*14*−*16*). In contrast, a basic N-terminal extension of the yeast HMGB homologue NHP6A is required for stable complex formation on both linear DNA and DNA minicircles, and basic C-terminal extensions stabilize binding of HMG-D and LEF-1 by binding in the major groove opposite the distorted minor groove (*3*, *17*, *18*). Thomsen et al. showed that interactions of the basic N-terminal and acidic C-terminal domains of maize HMGB1 may contribute to regulation of DNA interactions, and a similar phenomenon was observed for *Arabidopsis* HMGB1 and HMGB4 (*19*). This led the authors

† Supported by the National Science Foundation (Grant MCB-0414875 to A.G.) and by a Howard Hughes Medical Institute grant through the Undergraduate Biological Sciences Education Program to Louisiana State University.

* To whom correspondence should be addressed: Department of Biological Science, Louisiana State University, Baton Rouge, LA 70803. Telephone: (225) 578-5148. Fax: (225) 578-8790. E-mail: agrove@lsu.edu.

‡ Current address: University of Colorado Health Sciences Center, Denver, CO 80262.

§ These authors contributed equally to this work.

|| Current address: Walter Reed Army Institute of Research, Silver Spring, MD 20910.

[1] Abbreviations: HMG, high-mobility group; EMSA, electrophoretic mobility shift assay; CD, circular dichroism; T_m, melting temperature; $[\Theta]_{MRW}$, mean residue molar ellipticity.

10.1021/bi0522798 CCC: $33.50
Published on Web 02/21/2006

to argue that interaction of the variable terminal domains of plant HMGB proteins could serve as a molecular mechanism involved in the fine-tuning of the functional properties of these architectural proteins, depending on the structural requirements of specific nucleoprotein complexes.

Saccharomyces cerevisiae contains four HMGB homologues; NHP6A and -B, which contain a single HMG box, and HMO1 and -2, which more closely resemble vertebrate homologues by having two domains in the positions corresponding to box A and box B. For HMO1, the box A domain diverges significantly from HMG consensus sequences and is not predicted to adopt the classical HMG fold, while box B conforms more closely to the consensus. These two domains are followed by ~60 residues characterized by a lysine-rich C-terminus. HMO1 appears to be involved in the maintenance of chromatin integrity, as indicated by enhanced plasmid loss rates and nuclease-sensitive chromatin in *hmo1* knockout strains (*20*). HMO1 has also been shown to participate in mutagenesis control and in regulation of rDNA transcription (perhaps serving a function akin to that of mammalian UBF which contains six HMG domains) and to interact with the peptidyl-prolyl *cis-trans* isomerase FKBP12 (*21*−*23*). We have previously described the contribution of both box A and box B to DNA binding in vitro (*24*). We are reporting here the roles of each domain in DNA binding and bending. In contrast to classical two-HMG box proteins, our data suggest that box A and box B do interact with each other and that the basic C-terminal tail primarily interacts with box A. Surprisingly, the basic tail does not increase the DNA binding affinity for either linear or four-way junction DNA but is required for DNA bending by HMO1.

MATERIALS AND METHODS

Cloning and Purification of Proteins. Cloning of HMO1 and HMO1-boxA into pET28b for expression with an N-terminal His_6 tag was reported previously (*24*). Using a PCR-based site-directed mutagenesis approach with pET28b-HMO1 as a template, as described for generation of HMO1-boxA (*24*), the codon specifying Ala210 was replaced with a stop codon to create pET28b-HMO1-boxAB, carrying the gene encoding the truncated protein HMO1-boxAB using the forward primer 5′-TTACAGCACGCCTGAGAACCTC-CT-3′ (stop codon underlined) and the reverse primer 5′-ACTGAAAGGAATTGGAACCGGCGCAT-3′. DNA encoding HMO1-boxBC was amplified from pET28b-HMO1 using the forward primer 5′-GATCCACATATGCCAAA-GAAG-3′ and the reverse primer 5′-ATCCGGATATAGT-TCCTCCTT-3′, where an NdeI site (underlined) introduces a methionine in place of Ala105. To create plasmid pET5a-HMO1-boxBC, the amplified DNA was digested with NdeI and cloned into pET5a. Using PCR-based site-directed mutagenesis with pET5a-HMO1-boxBC as a template and the same primers that were used for generation of pET28b-HMO1-boxAB, the residue corresponding to the original Ala210 was replaced with a stop codon to create pET5a-HMO1-boxB.

Purification of N-terminally His_6-tagged HMO1 and HMO1-boxA was performed as described previously (*24*). Plasmids carrying genes encoding the remaining HMO1 domains were transformed into *Escherichia coli* Rosetta Blue. Cultures were grown to an A_{600} of ~0.4, and expression was induced with 1 mM isopropyl β-D-thiogalactopyranoside (IPTG) for 3 h. For purification of N-terminally His_6-tagged HMO1-boxAB, cells were pelleted, resuspended in dialysis/lysis buffer at pH 7 [50 mM $Na_xH_yPO_4$, 300 mM NaCl, 10 mM imidazole, 10% glycerol, 1 mM 2-mercaptoethanol, and 1 mM phenylmethylsulfonyl fluoride (PMSF)], and disrupted by sonication. Nucleic acids were digested by addition of DNase I followed by a 1 h incubation on ice. The lysate was supplemented with EDTA-free Complete (Roche Diagnostics) and passed through a nickel−nitrilotriacetic acid column equilibrated with dialysis/lysis buffer and washed with 5 column volumes of wash buffer at pH 7 (50 mM $Na_xH_yPO_4$, 300 mM NaCl, 20 mM imidazole, 10% glycerol, 1 mM 2-mercaptoethanol, and 1 mM PMSF). Proteins were eluted with a 50 mL linear gradient from 20 mM imidazole (wash buffer) to 250 mM imidazole (elution buffer, 50 mM $Na_xH_yPO_4$, 300 mM NaCl, 250 mM imidazole, 10% glycerol, 1 mM 2-mercaptoethanol, and 1 mM PMSF) followed by 100 mL of elution buffer.

For purification of untagged HMO1-boxBC, cells were resuspended in lysis buffer [50 mM Tris-HCl (pH 8.0), 1 M NaCl, 5% glycerol, 5 mM EDTA, 1 mM 2-mercaptoethanol, and 1 mM PMSF]. Cells were disrupted by sonication and nucleic acids digested by addition of DNase I followed by a 1 h incubation on ice. The extract was clarified by centrifugation at 5000*g* for 20 min. Cell lysates were dialyzed against HA buffer at pH 8.8 (20 mM Tris-HCl, 50 mM KCl, 10% glycerol, 1 mM EDTA, 4 mM 2-mercaptoethanol, and 1 mM PMSF). The dialysate was passed through tandem columns of DEAE-cellulose and CM-Sepharose equilibrated with the same buffer. HMO1-boxBC was eluted with a 100 mL linear gradient from 50 mM KCl (HA buffer) to 1 M KCl [HB buffer; 20 mM Tris-HCl, 1 M KCl, 10% glycerol, 1 mM EDTA, and 4 mM 2-mercaptoethanol, supplemented with one tablet of EDTA-free Complete (Roche Diagnostics)]. Peak fractions were judged to be >95% pure by Coomassie Blue-stained SDS−PAGE gels. For purification of untagged HMO1-boxB, cells were lysed as described for HMO1-boxBC, and cell lysates were dialyzed against HA buffer at pH 8.3. The dialysate was purified on heparin−agarose beads, and peak fractions eluted with a gradient from 50 mM KCl (HA buffer) to 1 M KCl (HB buffer at pH 8.3) were pooled and dialyzed against HA buffer at pH 7.0 (replacing Tris-HCl with 50 mM $Na_xH_yPO_4$) and passed through a heparin−agarose column equilibrated with the same buffer; >95% pure HMO1-boxB was eluted and analyzed as described above. Purified proteins were quantitated on Coomassie Blue-stained SDS−PAGE gels using bovine serum albumin as a standard. Cross-linking in solution was performed by incubation of 0.5 μg of protein with 1-ethyl 3-[3-(dimethylamino)propyl]carbodiimide (EDAC, prepared fresh as a 10 mg/mL solution in water) for 30 min at room temperature or with 0.1% glutaraldehyde for 10−30 min followed by analysis of cross-linked products on SDS−PAGE gels.

Circular Dichroism Spectroscopy. CD spectra were recorded on an AVIV model 202 CD spectrophotometer using a 1 cm path length sample cell. Wavelength scans from 200 to 240 nm were performed in triplicate, and data points were averaged and smoothed using standard methods. The wavelength scan shown for HMO1 was recorded at 25 °C with a protein concentration of 0.007 mg/mL in buffer A [2.5 mM

$Na_xH_yPO_4$ (pH 7.0), 0.5% glycerol, and 10 mM NaCl]. The wavelength scan for HMO1-boxA was recorded at 4 °C with a protein concentration of 0.05 mg/mL in buffer B [1 mM Tris-HCl (pH 7.0), 0.03% Tween 20, 10% glycerol, and 2.8 mM KCl].

The thermal stability of HMO1, HMO1-boxA, HMO1-boxAB, HMO1-boxBC, and HMO1-boxB was measured using the AVIV model 202 CD spectrophotometer and a 1 cm path length sample cell. HMO1, HMO1-boxAB, HMO1-boxBC, and HMO1-boxB were diluted to 0.025 mg/mL in CD buffer [50 mM $Na_xH_yPO_4$ (pH 8.0), 10% glycerol, 200 mM NaCl, and 0.05% Tween 20]. HMO1-boxA was diluted to 0.05 mg/mL in CD buffer. Thermal denaturation of HMO1 and HMO1-boxAB was also assessed in CD buffer at pH 7.0 (Tween 20 was omitted for HMO1). Temperature-dependent ellipticity measurements from 221 to 224 nm were recorded from 4 to 90 °C (2 °C intervals), and wavelength scans from 200 to 240 nm were obtained at 4 and 90 °C to assess secondary structure and confirm the folded and unfolded states. Reverse scans were performed at the same wavelengths from 90 to 4 °C (0.5 °C intervals) to assess the reversibility of unfolding. Ellipticity measurements were corrected for buffer effects. For all proteins except HMO1-boxAB, plots of the ellipticity values from 221 to 224 nm versus the corresponding temperatures were fit to a two-state model for protein denaturation (*25*). For HMO1-boxAB and HMO1 at pH 7.0, the plateau between the two transitions of the biphasic melting curve was estimated visually, and the plots were divided into single-transition plots to allow fitting to the two-state model. Fits were performed using KaleidaGraph. Melting temperatures (T_m) and the error of the fits are reported using the ellipticity measurements at 222 nm. All experiments were performed at least in duplicate.

Electrophoretic Mobility Shift Assays. Oligonucleotides were purchased and purified by denaturing gel electrophoresis. Four-way junctions were constructed and their integrities confirmed as we described previously (*24*). Briefly, the four-way junction was prepared by annealing the four strands, followed by purification of the junctions on native polyacrylamide gels. To ensure that all oligonucleotides were present, aliquots of the purified junctions were run on denaturing gels. EMSAs were performed as described previously (*24*) with 5 fmol of ^{32}P-labeled DNA and varying amounts of HMO1 variants. Complexes were resolved on prerun 7% (w/v) native polyacrylamide gels (39:1 acrylamide:bisacrylamide) at 4 °C with 0.5× TBE (50 mM Tris borate and 1 mM EDTA). Quantitation was performed on an Amersham Biosciences Storm Phosphorimager using software supplied by the manufacturer. The fraction of bound relative to total DNA was plotted as a function of protein concentration and fitted to the microscopic Hill equation bound/total $= \{m[1/(K_d^{n_H})(L)^{n_H}]\}/[1 + (1/K_d^{n_H})(L)^{n_H}]$, where m represents maximal saturation, to obtain the microscopic Hill K_d, reflecting half-maximal saturation of the DNA (the aggregate affinity for the DNA probe), and the Hill coefficient (n_H). Note that the aggregate affinities do not reflect actual binding constants for the reactions composed of several equilibria, each characterized by individual binding constants, and are only semiquantitative comparisons. Fits were performed using KaleidaGraph, and the quality of the fits was evaluated by visual inspection, χ^2 values, and correlation coefficients. All experiments were performed at least in triplicate, and values are reported as the mean ± the standard deviation.

To generate 26 or 18 bp duplex DNA, complementary oligonucleotides were mixed at equimolar concentrations, heated at 90 °C, and slowly cooled to room temperature. The sequence of the 26 bp duplex was 5′-CGTGACTACT-GTAAGTCGATGATCCG-3′, and that of the 18 bp DNA was 5′-CCTAGGCTACACCTACTC-3′. EMSAs were performed as described above with 5 fmol of DNA. Data were quantitated as described above and fitted to the microscopic Hill equation. All experiments were performed at least in triplicate, and values are reported as the mean ± the standard deviation.

For competition assays involving DNA minicircles, pET5a was digested with BspHI to generate a 105 bp fragment. The DNA was 5′-end labeled with T4 polynucleotide kinase, and intramolecular ligation was accomplished by incubation with T4 DNA ligase and *Thermotoga maritima* HU for 2 h at room temperature (*26*). Linear DNA was removed by treating the sample with exonuclease III for 1 h at room temperature, followed by purification of cyclized DNA on a 6% (w/v) native polyacrylamide gel. EMSAs were performed as described above with 5 fmol of DNA. For competition, cyclized 105 bp DNA and HMO1 were incubated for 30 min followed by addition of the indicated amount of supercoiled pUC18.

For EMSAs with phosphorylated proteins, 15 pmol of HMO1 variants was incubated with 500 units of tetrameric CKII (New England Biolabs) and 2 mM ATP in the buffer supplied by the manufacturer for 1 h at room temperature. Parallel reactions were performed without ATP. Proteins were diluted to the indicated concentrations and incubated with 5 fmol of four-way junction DNA, and reactions were resolved and visualized as described above. Confirmation of phosphorylation was performed by including [γ-^{32}P]ATP in the reactions, followed by analysis on SDS−PAGE gels. Gels were stained with Coomassie Blue for identification of protein, and phosphorylation was detected by phosphoimaging.

Ligase-Mediated Cyclization. Ligation substrates were prepared by digestion of pET5a with BspHI to generate a 105 bp fragment. DNA was 5′-end-labeled with T4 polynucleotide kinase and [γ-^{32}P]ATP. Reactions were initiated by addition of 20 units of T4 DNA ligase to a final volume of 100 μL of reaction buffer [20 mM Tris-HCl (pH 8), 50 mM NaCl, 10 mM $MgCl_2$, 0.1 mM Na_2EDTA, 1 mM DTT, and 0.05% BRIJ58] containing 1200 fmol of DNA, with or without the protein. Time points were taken at intervals of 30 min. For each time point, 8 μL of the reaction mixture was quenched by addition of 5 μL of stop buffer [75 mM EDTA, 15% glycerol, 0.1% bromophenol blue (BPB), 0.1% xylene cyanol, and 6 μg/μL proteinase K]. Samples were heated at 55 °C for 15 min and resolved on prerun 7% (w/v) native polyacrylamide gels (39:1 acrylamide:bisacrylamide) at 4 °C with 0.5× TBE. Cyclized DNA was identified by its resistance to digestion with exonuclease III. Ligation products were visualized by phosphorimaging.

RESULTS

Design of HMO1 Variants. For analysis of domain functions and domain−domain interactions in HMO1, we

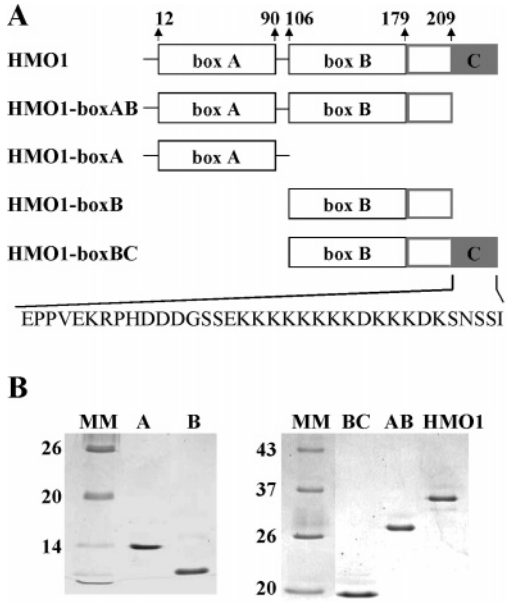

FIGURE 1: Domain organization of HMO1. (A) HMO1 is composed of HMG domains box A and box B, followed by a lysine-rich C-terminal extension (C). Truncated HMO1 variants analyzed in this work are listed. (B) HMO1 variants were purified to >95% homogeneity. Purified proteins, HMO1-box A (lane A) and HMO1-boxB (lane B), were analyzed on a 15% SDS−PAGE gel (left panel), and HMO1-boxBC (lane BC), HMO1-boxAB (lane AB), and the full-length protein were analyzed on a 12% gel (right panel). Molecular mass markers are given at the left (in kilodaltons).

generated several truncated variants. HMO1-boxA spans the short (11 amino acids) basic N-terminal extension, residues Ala12−Ala90, comprising the HMG-like domain, and the basic interdomain linker (residues Pro91−Ala105). HMO1-boxB starts at Pro106, the first residue of the box B HMG domain which ends at Leu179, and includes residues Glu180−Ala209 of the C-terminal extension; the remaining residues of the C-terminal tail comprise the lysine-rich sequence. HMO1-boxBC includes box B and the entire C-terminal tail, while HMO1-boxAB is deleted only for the lysine-rich segment. All proteins were purified to apparent homogeneity (Figure 1). DNA binding by untagged and N-terminally His_6-tagged HMO1 was previously compared, and the tag was found not to modulate DNA interaction (*24*). Experiments reported here were performed with His_6-tagged HMO1, HMO1-boxAB, and HMO1-boxA, while HMO1-boxBC and HMO1-boxB were untagged.

Potential association in solution between HMO1-boxA and HMO1-boxB was analyzed by chemical cross-linking using carbodiimide which activates carboxyl groups for direct amide bonding to primary amino groups; this reagent was chosen as the theoretical pI of box A is 4.1. While some dimerization of HMO1-boxA was seen (consistent with the previously reported ability of HMO1 to self-associate; *21*), no cross-linking of HMO1-boxA to HMO1-boxB (whether the lysine-rich tail was present) was detectable (data not shown). Similar results were obtained when glutaraldehyde was used for cross-linking (of lysines). However, this does not exclude interaction between these domains, as only species properly oriented for the reagent to react will be captured.

Interaction with Linear and Four-Way Junction DNA. DNA binding by HMO1 variants was analyzed using electrophoretic mobility shift assays (EMSAs). While HMO1 forms two detectable complexes with 26 bp DNA under these conditions (Figure 2A), HMO1-boxA fails to associate stably (not shown and ref *24*). Surprisingly, removal of the lysine-rich tail results in formation of a more stable complex by HMO1-boxAB and a distinct migration pattern of complexes (Figure 2B). Fits of fractional complex formation to the Hill equation suggest positive cooperativity and little difference in affinity between HMO1 and HMO1-boxAB (half-maximal saturation at 26.5 and 31.9 nM, respectively; Table 1). While Scatchard plots show curvature consistent with positive cooperativity (not shown), we note that as the total length of the DNA is relatively short, apparent negative cooperativity is seen at higher protein concentrations as it becomes increasingly difficult to saturate the DNA probe (a statistical effect, not necessarily reflecting modification of adjacent binding sites). The "competing" effects of cooperativity of protein binding and end effects associated with the length of the DNA probe require that the reported Hill coefficients be considered qualitative comparisons. As reported previously, HMO1 has only a modest preference for four-way junction DNA compared to the linear duplex (half-maximal saturation at 10.4 nM; Figure 3A and Table 1) (*24*). This modest preference is also exhibited by HMO1-boxAB (half-maximal saturation at 18.4 nM; Figure 3B).

Removal of the box A domain and the interdomain linker to generate HMO1-boxBC results in a modest decrease in affinity for linear 26 bp DNA (half-maximal saturation at 50.3 nM; Figure 2C) but retention of a pattern of complexes similar to that seen for full-length HMO1. In contrast, the additional truncation of the lysine-rich tail to generate HMO1-boxB appears to change the stoichiometry of binding to 26 bp DNA, although no change in the overall affinity is evident (half-maximal saturation at 54.5 nM; Figure 2D). This change in the stoichiometry of binding is particularly evident with four-way junction DNA, with which both HMO1-boxBC and HMO1-boxB, in particular, form numerous complexes (Figure 3C,D). Both proteins bind preferentially to four-way junctions compared to linear DNA, with

Table 1: HMO1 Variants[a]

	$[\Theta]_{MRW}$	T_m (°C)	K_d(26 bp)	n_H	K_d(4WJ)	n_H
HMO1	−17693	47.9 ± 0.1	26.5 ± 1.1	1.6 ± 0.1	10.4 ± 0.5	1.8 ± 0.2
HMO1-boxAB	−14542	46.0 ± 0.4 63.3 ± 0.5	31.9 ± 1.1	2.4 ± 0.2	18.4 ± 0.5	2.5 ± 0.2
HMO1-boxA	−11206	57.2 ± 0.1	nc[b]		nd[c]	
HMO1-boxB	−14687	47.2 ± 0.1	54.5 ± 2.9	1.1 ± 0.1	14.4 ± 0.3	3.3 ± 0.2
HMO1-boxBC	−13469	46.1 ± 0.1	50.3 ± 3.0	1.0 ± 0.1	10.1 ± 0.4	1.8 ± 0.1

[a] The mean residue molar ellipticity ($[\Theta]_{MRW}$) is reported at 222 nm and 4 °C (degrees square centimeter per decimole). The Hill K_d (in nanomolar) represents half-maximal saturation of the DNA probe, and n_H is the Hill coefficient. [b] No complex. [c] Not determined (low-affinity binding leading to overly rapid complex dissociation during electrophoresis for reliable determination).

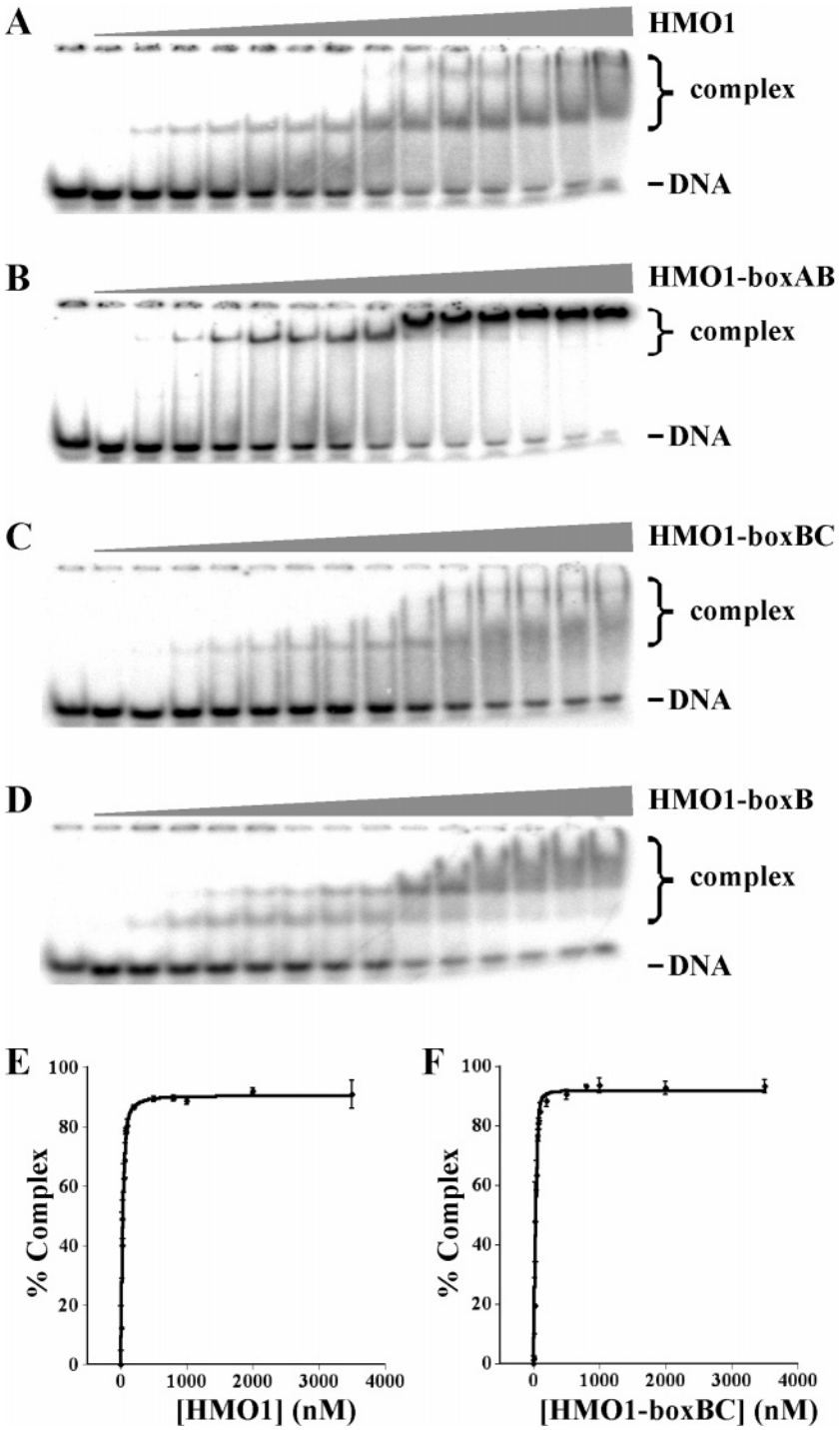

FIGURE 2: Electrophoretic analysis of 26 bp DNA titrated with HMO1 variants. Reaction mixtures contained 5 fmol of DNA and increasing concentrations of HMO1 (A), HMO1-boxAB (B), HMO1-boxBC (C), or HMO1-boxB (D). Free DNA and complexes are identified at the right. Reaction mixtures in lane 1 contained DNA only. Reaction mixtures in lanes 2−15 contained 10, 20, 30, 45, 65, 80, 100, 200, 500, 800, 1000, 2000, 3500, and 7500 nM protein, respectively (panels A and B), or 10, 25, 50, 75, 100, 125, 150, 200, 500, 1000, 2000, 3000, 4000, and 6000 nM protein, respectively (panels C and D). (E and F) Binding isotherms for binding of HMO1 and HMO1-boxBC to 26 bp DNA. When error bars are not shown, they are smaller than the size of the symbol.

half-maximal saturation at 10.1 and 14.4 nM, respectively. While the overall affinity of the HMO1 variants appears to change little upon removal of box A, the stoichiometry of binding changes appreciably, consistent with a contribution of box A to DNA interaction. Removal of the lysine-rich tail from HMO1-boxBC primarily results in formation of additional retarded species, while its removal from HMO1 results in formation of a more stable complex, particularly with linear DNA.

HMO1 was previously shown to exhibit a longer residence time on DNA minicircles compared to linear or supercoiled DNA (*24*). While HMO1-boxAB exhibits a distinct pattern of complex formation with DNA minicircles, the lysine-rich tail appears not to be required for preferred binding to the minicircle DNA, as evidenced by the inability of supercoiled plasmid DNA to compete effectively for binding (Figure 4, top panels). In contrast, both HMO1-boxB and HMO1-boxBC are more effectively forced off the minicircle by

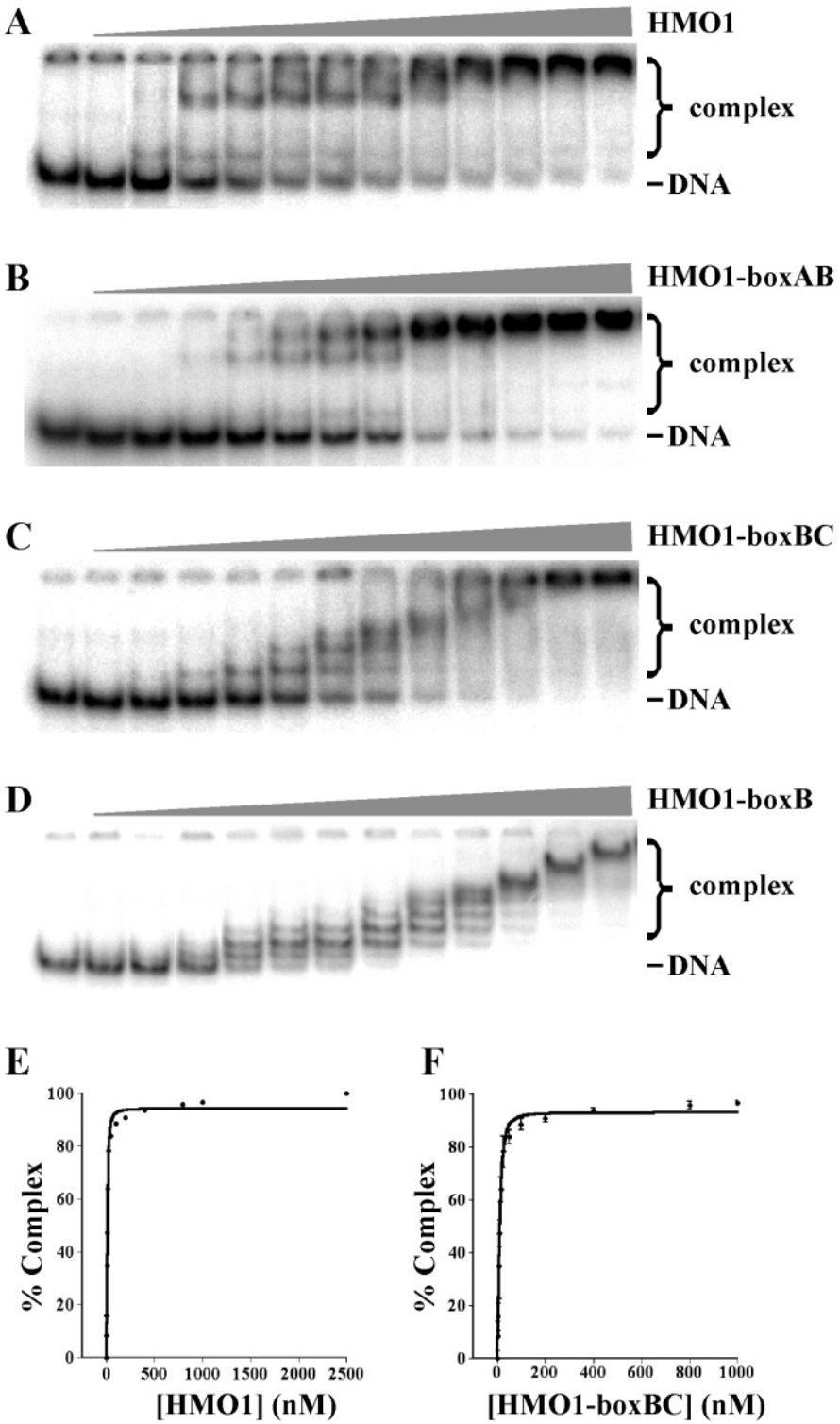

FIGURE 3: Electrophoretic analysis of four-way junction DNA titrated with HMO1 variants. Reaction mixtures contained 5 fmol of DNA and increasing concentrations of HMO1 (A), HMO1-boxAB (B), HMO1-boxBC (C), or HMO1-boxB (D). Free DNA and complexes are identified at the right. Reaction mixtures in lane 1 contained DNA only. Reaction mixtures in lanes 2−13 contained 5, 7.5, 10, 15, 20, 25, 30, 50, 100, 200, 400, and 800 nM protein, respectively (panels A and B), 5, 7.5, 10, 15, 25, 50, 100, 200, 400, 800, and 1000 nM protein, respectively (panel C), or 5, 7.5, 10, 12.5, 15, 17.5, 20, 30, 60, 100, 200, 500, and 1000 nM protein, respectively (panel D). (E and F) Binding isotherms for binding of HMO1 and HMO1-boxBC to four-way junction DNA. When error bars are not shown, they are smaller than the size of the symbol.

addition of supercoiled DNA, indicating that box A is required for preferred binding to the constrained minicircle (bottom panels).

Box A and the C-Terminal Tail Are Required for DNA Bending. DNA bending was assessed using a ligase-mediated cyclization assay in which 105 bp DNA was cyclized with T4 DNA ligase in the presence of HMO1 variants. HMO1 promotes the formation of constrained minicircles, as evidenced by their resistance to digestion with exonuclease III, an indication of its ability to bend the DNA duplex (Figure 5, top left panel). Notably, the ability to bend DNA is effectively abolished with removal of the lysine-rich tail

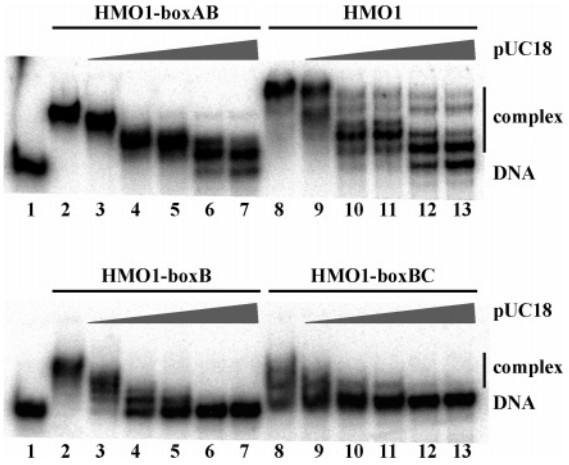

FIGURE 4: Box A domain that is required for preferred binding to circular DNA. Five femtomoles of cyclized 105 bp DNA was incubated with the indicated HMO1 variant (500 nM) followed by addition of supercoiled pUC18. Reaction mixtures in lane 1 contain no HMO1. Reaction mixtures in lanes 2 and 8 contain no competitor DNA (pUC18). Reaction mixtures in lanes 3−7 and 9−13 contain 1, 5, 10, 50, and 100 fmol of pUC18, respectively.

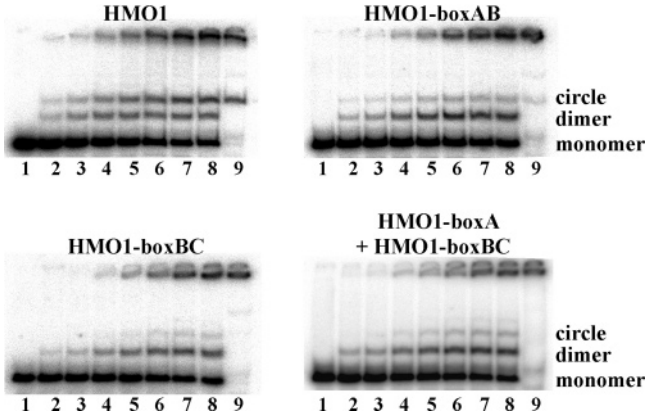

FIGURE 5: Time course ligation of 105 bp DNA. DNA was incubated with the indicated HMO1 variants (50 nM) and T4 DNA ligase. Lane 1 contained no ligase. Lanes 2−8 represent time points taken at 0.5, 1, 2.5, 5, 10, 20, and 30 min, respectively. Reaction mixtures in lane 9 were incubated with ligase for 30 min followed by treatment with exonuclease III for 30 min.

(HMO1-boxAB, top right panel) or box A (HMO1-boxBC, bottom left panel); the monomeric circle comigrates with the linear trimer, as evidenced also by the observation that cyclization of 105 bp DNA in the absence of any HMO1 fragment produces this exonuclease III-sensitive species (*24*). No DNA cyclization was seen in the presence of HMO1-boxB or HMO1-boxA (not shown). The failure of HMO1-boxA and HMO1-boxBC to assemble into a functional conformation is evidenced by the inability to restore DNA bending after co-incubation of the two fragments (bottom right panel). Evidently, DNA bending by HMO1 requires the presence of both box A and the lysine-rich tail in a single polypeptide.

Thermal Stability of HMO1 Domains. DNA cyclization assays raise the possibility that an interaction between box A and the C-terminal tail is required for functional activity. We therefore further explored domain−domain interactions by circular dichroism (CD) spectroscopy. All proteins were found to exhibit significant α-helical content as evidenced by negative ellipticities at 208 and 222 nm (ref *24* and data not shown). To measure thermal stability, ellipticity measurements at four wavelengths spanning the negative ellipticity minimum of 222 nm were recorded over the temperature range of 4−90 °C and fitted to a modified van't Hoff equation for a two-state unfolding equilibrium (Figure 6). At 4 °C, the amplitude of the negative mean residue molar ellipticity ($[\Theta]_{MRW}$) at 222 nm is comparable for HMO1-boxAB, HMO1-boxB, and HMO1-boxBC; that of full-length HMO1 is significantly greater, and the amplitude of $[\Theta]_{MRW}$ for HMO1-boxA is lower (Table 1). These variations suggest distinct secondary structure content. The CD melting curve for full-length HMO1 reveals a sharp, single transition from the native to a definitive denatured conformation with a calculated melting temperature (T_m) of 47.9 °C, suggesting a two-state unfolding equilibrium. For the individual box A and box B domains, two-state unfolding transitions were also seen, with T_m values of 57.2 and 47.2 °C, respectively, while HMO1-boxBC melts at 46.1 °C. The comparable unfolding transitions of HMO1-boxB and HMO1-boxBC may imply little interaction between box B and the lysine-rich tail, while the markedly higher T_m for HMO1-boxA compared to that of full-length HMO1 suggests that interactions between box A and box B or between box A and the lysine-rich tail induce a less stable conformation of box A. In contrast, HMO1-boxAB, truncated for the lysine-rich extension, exhibits a biphasic transition from the native to the denatured state with T_m values of 46.0 and 63.3 °C, consistent with the presence of two distinct domains and suggesting that the destabilization of box A seen in full-length HMO1 is primarily due to interactions between box A and the tail. Two unfolding transitions were also observed for HMO1-boxAB at pH 7.0 (T_m values of 48.2 ± 2.0 and 71.7 ± 0.7 °C; not shown). Notably, HMO1 also exhibited biphasic unfolding at pH 7.0 with T_m values of 23.5 ± 0.4 and 57.6 ± 0.8 °C (Figure 6, bottom right panel). As discussed below, the low-temperature transition is most likely due to unfolding of the C-terminal tail. While some secondary structure was seen on refolding of the proteins, the original secondary structure was not recovered, as judged by wavelength scans (not shown).

Phosphorylation Modulates Domain−Domain Interactions. HMGB proteins have been reported to serve as substrates for casein kinase II (CKII) (*19*, *27*−*29*). Analysis of the HMO1 sequence using Scansite, which predicts optimal phosphorylation sites for specific protein Ser/Thr kinases using a matrix of selectivity values for amino acids at each position relative to the phosphorylation site (*30*, *31*), predicts two sites for CKII. One site, Ser153, is located in box B, in the loop between helices II and III (Figure 7), while the other is in the C-terminal tail (Ser225). We used this information as an additional tool to monitor interactions between domains. HMO1 is indeed a substrate for CKII (Figure 8A), and phosphorylation of all fragments except HMO1-boxA is seen; phosphorylation reduces the positive charge and causes a faster migration compared to that of the unphosphorylated protein (compare Figures 1B and 8A). The observed difference in migration is therefore what would be expected. Second, Coomassie staining of the gels confirms that the stained bands correspond to those identified by phosphorimaging (not shown), arguing against the existence of labeled contaminants (as none of the protein preparations contain abundant contaminants, Figure 1). We also note that a single labeled species is seen for HMO1-boxB (band 5),

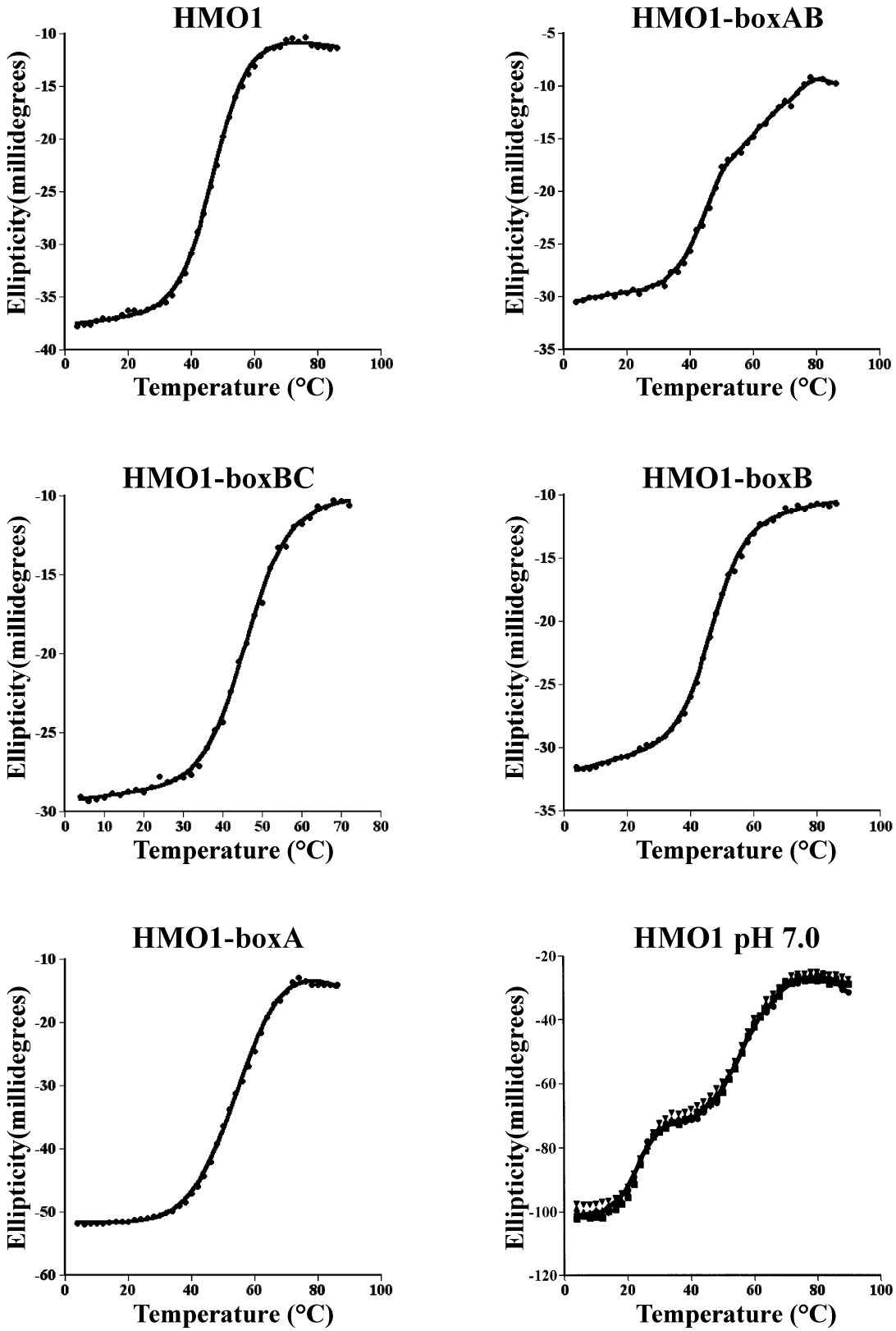

FIGURE 6: Thermal unfolding transitions of HMO1 variants. Ellipticity measurements were collected from 4 to 90 °C at four wavelengths (221−224 nm) spanning the negative ellipticity maximum characteristic of α-helices; results recorded at pH 8.0 and 222 nm are shown for all variants. The bottom right panel shows thermal unfolding at all four wavelengths of 0.06 mg/mL HMO1 recorded at pH 7.0.

while two bands appear for HMO1-boxBC (bands 4 and 5). As HMO1-boxB is certainly at least monophosphorylated to be detectable by phosphorimaging, HMO1-boxBC must carry at least one additional phosphate to compensate for the difference in migration of the unphosphorylated proteins (Figure 1). Likewise, a single phosphorylated species is detected for HMO1-boxAB (band 3), while HMO1 is phosphorylated at two sites [bands 2 and 3; the doubly phosphorylated HMO1 and singly phosphorylated HMO1-boxAB comigrate with the autophosphorylated 26 kDa CKII

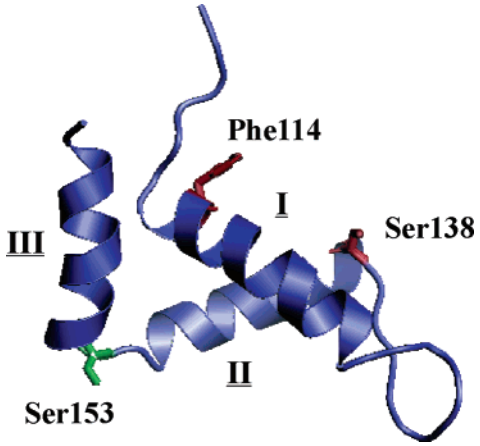

FIGURE 7: Model of box B generated with SwissModel. A predicted phosphorylation site in the loop between helices II and III is colored green. Residues colored red are predicted to contact DNA. Helices are identified with Roman numerals. This illustration was generated with PyMol.

subunit, as shown by Coomassie staining of SDS−PAGE gels (not shown); the level of phosphorylation of CKII subunits is reduced in the presence of an exogenous substrate]. The simplest explanation is therefore that the observed phosphorylated species correspond to phosphorylation at the predicted sites, one in box B and one in the C-terminus.

Analysis of DNA binding shows that phosphorylation of HMO1-boxB has no effect (Figure 8B), while the extent of DNA binding by the other phosphorylated HMO1 variants is reduced (Figure 8C−E), as indicated by a lower fractional saturation of the DNA probes with the phosphorylated HMO1 variant. The location of Ser153 opposite the DNA-binding interface of box B (Figure 7) is consistent with phosphorylation of HMO1-boxB having no effect on DNA binding. The reduced level of DNA binding seen for phosphorylated HMO1-boxBC therefore suggests that phosphorylation of the C-terminus causes the observed effect, and that the C-terminus contacts DNA or the DNA-binding interface of box B. Notably, phosphorylated HMO1-boxAB also exhibits a reduced level of DNA binding. As DNA binding by the isolated box B domain is unaffected by phosphorylation, we interpret the weakened DNA interaction of phosphorylated HMO1-boxAB in terms of attenuated interactions between boxes A and B.

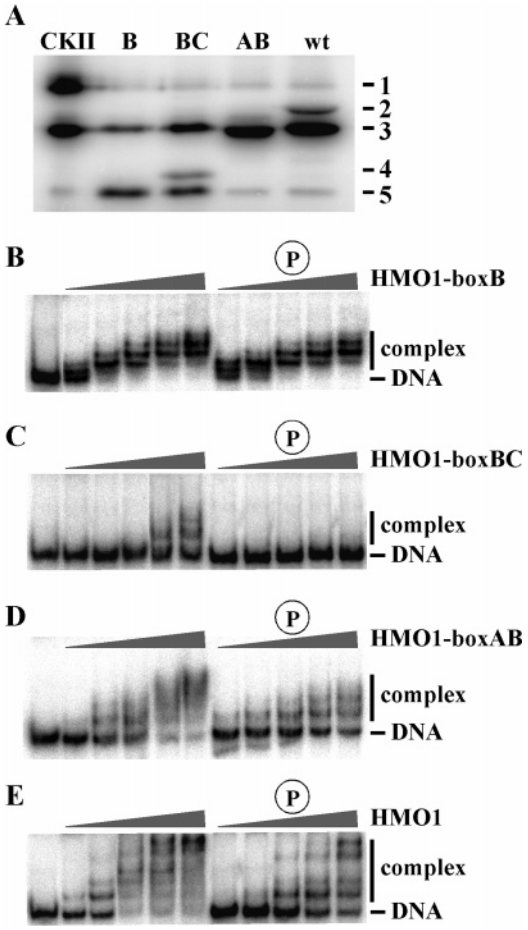

FIGURE 8: HMO1 variants phosphorylated by casein kinase II. (A) SDS−PAGE gel showing phosphorylation of HMO1-boxB (B), yielding a single phosphorylated species identified as band 5, HMO1-boxBC (BC), resulting in two species marked 4 and 5, HMO1-boxAB (AB) comigrating with the autophosphorylated CKII subunit (marked 3), and HMO1 (wt), yielding two phosphorylated species marked 2 and 3. HMO1-boxA is not a substrate for CKII. Lane 1 contained CKII only, with bands marked 1 and 3 representing autophosphorylated 26 and 44 kDa subunits, respectively. (B) DNA binding by phosphorylated HMO1 variants. EMSA with 5 fmol of four-way junction DNA and the indicated HMO1 variant. Results with the unphosphorylated protein are shown in the left panels and results with the phosphorylated protein in the right panels. Reaction mixtures in lane 1 contained no protein. Protein concentrations, identical for all panels, are 12.5, 25, 50, 100, and 150 nM.

DISCUSSION

Domain−Domain Interactions in HMO1. While box B conforms to consensus HMG sequences, the sequence of box A differs from the consensus and includes a five-amino acid insertion in helix III. This insertion contains a helix-breaking glycine and may therefore alter the conformation of the folded domain, consistent with the lower amplitude of $[\Theta]_{MRW}$ for HMO1-boxA (Table 1). A different conformation is also consistent with the differential thermal stability. The comparable $[\Theta]_{MRW}$ for HMO1-boxAB and HMO1-boxB suggests that interactions between box A and box B (or the portion of the C-terminal fragment included in HMO1-boxB) increase the helical content of box A. A change in the conformation of box A on association with box B is also suggested by the increase in the T_m for the box A domain from ~57 to 63 °C (Figure 6). Assuming that HMO1 is indeed phosphorylated at the predicted sites, phosphorylation of HMO1-boxAB would occur in the loop connecting box B helices II and III; as this phosphorylation does not modulate DNA binding by HMO1-box B (Figure 8B), but attenuates DNA binding by HMO1-boxAB, we surmise that the observed interaction occurs between boxes A and B. Interactions between box A and box B are consistent with the theoretical pI of the isolated box A domain (excluding the N-terminal residues and the basic interdomain linker) of 4.1 and the pI of box B of 9.1. This observation is distinct from that for vertebrate HMGB1, for which no association between HMG domains was evident (*14*, *15*, *32*, *33*).

The lysine-rich segment of the C-terminal tail also associates with box A. This is evident from the significant decrease in the thermal stability of the box A domain in full-length HMO1 compared to that of HMO1-boxA or HMO1-boxAB (Figure 6). For HMO1, the good fit to a two-state

unfolding model is consistent with coupled melting of both domains. This evidently depends on the presence of the lysine-rich tail, as the melting transition for HMO1-boxAB is markedly different. The good fit to the two-state model also implies that no intermediate state is significantly populated during the thermal transition. A two-state unfolding mechanism was also reported for vertebrate HMGB1 (*14*, *34*).

We also note the increase in the magnitude of $[\Theta]_{MRW}$ for HMO1 compared to that of HMO1-boxAB which indicates conformational changes associated with inclusion of the lysine-rich tail. Since a comparable change in $[\Theta]_{MRW}$ is not associated with addition of the tail to HMO1-boxB (rather, the $[\Theta]_{MRW}$ reflects lower helical content for HMO1-boxBC), we conclude that interactions between box A and the tail are required for the observed conformational change. That the box A domain does not unfold independently in HMO1 is also indicated by the change in denaturation enthalpy between HMO1-boxA and the full-length protein ($\Delta H^\circ = 27$ kcal/mol for HMO1-boxA and 37 and 38 kcal/mol for HMO1 and HMO1-boxB, respectively).

When thermal denaturation of HMO1 and HMO1-boxAB was performed at pH 7.0, a main difference was the appearance of a separate denaturation event for HMO1 with a very low T_m of 23 °C (Figure 6). The lysine-rich tail would exhibit less charge repulsion at pH 8.0 than at pH 7.0; accordingly, this domain may fold more stably at pH 8.0, which is reflected in the greater amplitude of $[\Theta]_{MRW}$ for full-length HMO1 and its single unfolding transition (Table 1), but undergo a separate transition to the unfolded state at pH 7.0. While interactions between HMG boxes A and B and between box A and the lysine-rich tail are indicated from these analyses, the failure to restore DNA binding properties of full-length HMO1 by association of individual fragments suggests that proper association requires each domain to be encoded on a single polypeptide. This contrasts with HMGB1 for which a peptide representing the acidic C-terminus associates with the box AB fragment to restore the thermal stability seen for the full-length protein, suggesting assembly from isolated domains (*16*).

Mechanism of DNA Binding by HMO1. The box B domain of HMO1 contributes significant DNA binding affinity (Table 1). However, it is interactions between box A and the lysine-rich C-terminus that determine substrate specificity and DNA bending (Figures 4 and 5). Evidently, the mode of contact with DNA changes considerably with inclusion of the C-terminal tail, as shown by the differential complex stability and DNA bending by HMO1 and HMO1-boxAB. As discussed above, significant conformational changes occur in box A upon association with box B and the tail, and the C-terminal domain appears to fold only upon association with box A. In contrast, our data do not indicate significant changes in the conformation or dynamics of box B upon its association with other domains (both T_m and ΔH° are essentially unaltered for HMO1-boxB, HMO1-boxBC, and HMO1).

The HMG domain interacts with ~10 bp of the DNA duplex. This is consistent with the number of complexes seen on 26 bp DNA with the isolated box B domain (Figure 2). While an 18 bp duplex was previously shown not to support formation of a stable complex with full-length HMO1 (*24*), a single complex is seen with HMO1-boxAB (not shown); this indicates that both boxes A and B contact ~10 bp of the duplex and suggests that the additional complex seen with 26 bp DNA may involve only the higher-affinity box B interacting with the DNA and/or protein−protein contacts. The pattern of complexes on four-way junction DNA is consistent with preferential binding at the junction crossover, leading to a compact complex with high mobility, while additional complexes suggest progressive occupancy of the junction arms.

The HMG domain binds to the minor grove of DNA by partial intercalation of one or two surface-exposed, conserved hydrophobic residues into the base pair stack. For vertebrate HMGB1, the DNA-intercalating residues are located in helices I and II, and both can contribute to binding affinity. Our data show that HMO1, whose box B lacks the equivalent hydrophobic residue in helix II (Ser138, Figure 7), has a limited preference for distorted DNA. A modest preference for four-way junction DNA is also seen for HMO1-boxB. Structures of HMGB proteins in complex with four-way junction DNA or platinated DNA show that the helix II hydrophobic residue stacks on an exposed base pair and on the second guanosine of the cisplatin adduct, respectively (*35*−*39*). This results in a different disposition of the protein with regard to the DNA bend compared with that of sequence-specific proteins, e.g., SRY and LEF-1, whose primary DNA-intercalating residue is in helix I. Recently, it was also shown that NHP6A, which kinks duplex DNA using its helix I residue as the primary bending wedge, uses its helix II hydrophobic residue for selective recognition of cisplatin-modified DNA (*35*). An argument against the absolute requirement for a helix II hydrophobic residue for recognition of four-way junctions or platinated DNA is that SRY and LEF-1, which both have a polar residue at the equivalent position of helix II, retain high-affinity binding to both modified DNA constructs (*36*−*39*). The absence of a helix II bending wedge in box B may predict an orientation on DNA akin to that reported for SRY or LEF-1.

The effect of the lysine-rich tail on DNA binding is not what would be predicted from simple electrostatics, pointing to a change in the conformation or dynamics of the HMG box(es) upon association with the tail, and consistent with the observed changes in the secondary structure and stability of box A. Evidently, the role of the lysine-rich tail in bending is not based on affinity but is an intrinsic effect of the tail on the mechanism of bending; whether this mechanism involves direct contacts between the basic C-terminus and the DNA or is based solely on conformational changes in box A cannot be determined from these data. If box A is induced to adopt a HMG-like conformation, then it would possess potential intercalating bending wedges in both helices I (Leu) and II (Ile), consistent with its ability to bend DNA.

The data presented here suggest that the functional significance of the tripartite domain organization of HMO1 is the ability to modulate DNA bending without compromising complex stability. Our DNA binding experiments were performed at pH 8.0, where HMO1 is more stable. In vivo, a lower pH would be encountered, but molecular crowding and interaction with cellular macromolecules may serve to stabilize the protein compared to what is observed in dilute solution in vitro (Figure 6). We would therefore anticipate that the more stably folded conformation exists in vivo. However, as the C-terminal domain appears to be only

marginally stable at physiological pH and temperature, its conformation may potentially be readily modulated by covalent modification or by association with other cellular factors, leading to differential DNA bending. Such properties may explain the ability of HMO1 to serve as a general chromatin-associated factor involved in the maintenance of chromatin integrity by virtue of its long residence time on DNA and at the same time to serve as a specific architectural transcription factor in rDNA transcription.

REFERENCES

1. Bustin, M., and Reeves, R. (1996) High-mobility-group chromosomal proteins: Architectural components that facilitate chromatin function, *Prog. Nucleic Acid Res. Mol. Biol. 54*, 35−100.
2. Bustin, M. (1999) Regulation of DNA-dependent activities by the functional motifs of the high-mobility-group chromosomal proteins, *Mol. Cell. Biol. 19*, 5237−5246.
3. Love, J. L., Li, X., Case, D. A., Giese, K., Grosschedl, R., and Wright, P. E. (1995) Structural basis for DNA bending by the architectural transcription factor LEF-1, *Nature 376*, 791−795.
4. Hardman, C. H., Broadhurst, R. W., Raine, A. R., Grasser, K. D., Thomas, J. O., and Laue, E. D. (1995) Structure of the A-domain of HMG1 and its interaction with DNA as studied by heteronuclear three- and four-dimensional NMR spectroscopy, *Biochemistry 34*, 16596−16607.
5. Weir, H. M., Kraulis, P. J., Hill, C. S., Raine, A. R. C., Laue, E. D., and Thomas, J. O. (1993) Structure of the HMG box motif in the B-domain of HMG1, *EMBO J. 12*, 1311−1319.
6. He, Q., Ohndorf, U. M., and Lippard, S. J. (2000) Intercalating residues determine the mode of HMG1 domains A and B binding to cisplatin-modified DNA, *Biochemistry 39*, 14426−14435.
7. Jones, D. N. M., Searles, M. A., Shaw, G. L., Churchill, M. E. A., Ner, S. S., Keeler, J., Travers, A. A., and Neuhaus, D. (1994) The solution structure and dynamics of the DNA-binding domain of HMG-D from *Drosophila melanogaster*, *Structure 2*, 609−627.
8. Allain, F. H. T., Yen, Y. M., Masse, J. E., Schultze, P., Dieckmann, T., Johnson, R. C., and Feigon, J. (1999) Solution structure of the HMG protein NHP6A and its interaction with DNA reveals the structural determinants for non-sequence-specific binding, *EMBO J. 18*, 2563−2579.
9. Werner, M. H., Huth, J. R., Gronenborn, A. M., and Clore, G. M. (1995) Molecular basis of human 46X,Y sex reversal revealed from the three-dimensional solution structure of the human SRY-DNA complex, *Cell 81*, 705−714.
10. Ohndorf, U. M., Rould, M. A., He, Q., Pabo, C. O., and Lippard, S. J. (1999) Basis for recognition of cisplatin-modified DNA by high-mobility-group proteins, *Nature 399*, 708−712.
11. Jamieson, E. R., and Lippard, S. J. (1999) Structure, Recognition, and Processing of Cisplatin-DNA Adducts, *Chem. Rev. 99*, 2469−2498.
12. Thomas, J. O. (2001) HMG1 and 2: Architectural DNA-binding proteins, *Biochem. Soc. Trans. 29*, 395−401.
13. Lee, K. B., and Thomas, J. O. (2000) The effect of the acidic tail on the DNA-binding properties of the HMG1,2 class of proteins: Insights from tail switching and tail removal, *J. Mol. Biol. 304*, 135−149.
14. Ramstein, J., Locker, D., Bianchi, M. E., and Leng, M. (1999) Domain-domain interactions in high mobility group 1 protein (HMG1), *Eur. J. Biochem. 260*, 692−700.
15. Taudte, S., Xin, H., Bell, A. J., Jr., and Kallenbach, N. R. (2001) Interactions between HMG boxes, *Protein Eng. 14*, 1015−1023.
16. Knapp, S., Muller, S., Digilio, G., Bonaldi, T., Bianchi, M. E., and Musco, G. (2004) The long acidic tail of high mobility group box 1 (HMGB1) protein forms an extended and flexible structure that interacts with specific residues within and between the HMG boxes, *Biochemistry 43*, 11992−11997.
17. Yen, Y., Wong, B., and Johnson, C. R. (1998) Determinants of DNA binding and bending by the *Saccharomyces cerevisiae* high mobility group protein NHP6A that are important for its biological activities. Role of the unique N terminus and putative intercalating methionine, *J. Biol. Chem. 273*, 4430−4435.
18. Dow, L. K., Jones, D. N., Wolfe, S. A., Verdine, G. L., and Churchill, M. E. (2000) Structural studies of the high mobility group globular domain and basic tail of HMG-D bound to disulfide cross-linked DNA, *Biochemistry 39*, 9725−9736.
19. Thomsen, M. S., Franssen, L., Launholt, D., Fojan, P., and Grasser, K. D. (2004) Interactions of the basic N-terminal and the acidic C-terminal domains of the maize chromosomal HMGB1 protein, *Biochemistry 43*, 8029−8037.
20. Lu, J., Kobayashi, R., and Brill, J. S. (1996) Characterization of a high mobility group 1/2 homolog in yeast, *J. Biol. Chem. 271*, 33678−33685.
21. Dolinski, J. K., and Heitmain, J. (1999) Hmo1p, a high mobility group 1/2 homolog, genetically and physically interacts with the yeast FKBP12 prolyl isomerase, *Genetics 151*, 935−944.
22. Gadal, O., Labarre, S., Boschiero, C., and Thuriaux, P. (2002) Hmo1, an HMG-box protein, belongs to the yeast ribosomal DNA transcription system, *EMBO J. 21*, 5498−5507.
23. Alekseev, Y. S., Kovaltsova, V. S., Fedorova, V. I., Gracheva, M. L., Evstukhina, A. T., Peshekhonov, T. V., and Korolev, G. V. (2002) HSM2 (HMO1) gene participates in mutagenesis control in yeast *Saccharomyces cerevisiae*, *DNA Repair 1*, 287−297.
24. Kamau, E., Bauerle, K. T., and Grove, A. (2004) The *Saccharomyces cerevisiae* high mobility group box protein HMO1 contains two functional DNA-binding domains, *J. Biol. Chem. 279*, 55234−55240.
25. Ramsay, G. D., and Eftink, M. R. (1994) Analysis of multidimensional spectroscopic data to monitor unfolding of proteins, *Methods Enzymol. 240*, 615−645.
26. Grove, A., and Lim, L. (2001) High affinity DNA binding of HU protein from the hyperthermophile *Thermotoga maritima*, *J. Mol. Biol. 311*, 491−502.
27. Klimczak, L. J., and Cashmore, A. R. (1994) Microheterogeneous Cytosolic High-Mobility Group Proteins from Broccoli Co-Purify with and Are Phosphorylated by Casein Kinase II, *Plant Physiol. 105*, 911−919.
28. Wisniewski, J. R., Szewczuk, Z., Petry, I., Schwanbeck, R., and Renner, U. (1999) Constitutive phosphorylation of the acidic tails of the high mobility group 1 proteins by casein kinase II alters their conformation, stability, and DNA binding specificity, *J. Biol. Chem. 274*, 20116−20122.
29. Stemmer, C., Schwander, A., Bauw, G., Fojan, P., and Grasser, K. D. (2002) Protein kinase CK2 differentially phosphorylates maize chromosomal high mobility group B (HMGB) proteins modulating their stability and DNA interactions, *J. Biol. Chem. 277*, 1092−1098.
30. Songyang, Z., Blechner, S., Hoagland, N., Hoekstra, M. F., Piwnica-Worms, H., and Cantley, L. C. (1994) Use of an oriented peptide library to determine the optimal substrates of protein kinases, *Curr. Biol. 4*, 973−982.
31. Obenauer, J. C., Cantley, L. C., and Yaffe, M. B. (2003) Scansite 2.0: Proteome-wide prediction of cell signaling interactions using short sequence motifs, *Nucleic Acids Res. 31*, 3635−3641.
32. Grasser, K. D., Teo, S. H., Lee, K. B., Broadhurst, R. W., Rees, C., Hardman, C. H., and Thomas, J. O. (1998) DNA-binding properties of the tandem HMG boxes of high-mobility-group protein 1 (HMG1), *Eur. J. Biochem. 253*, 787−795.
33. Crane-Robinson, C., Read, C. M., Cary, P. D., Driscoll, P. C., Dragan, A. I., and Privalov, P. L. (1998) The energetics of HMG box interactions with DNA. Thermodynamic description of the box from mouse Sox-5, *J. Mol. Biol. 281*, 705−717.
34. Taudte, S., Xin, H., and Kallenbach, N. R. (2000) Alanine mutagenesis of high-mobility-group-protein-1 box B (HMG1-B), *Biochem. J. 347*, 807−814.
35. Wong, B., Masse, E. J., Yen, Y., Giannikoupolous, P., Feigon, J., and Johnson, C. R. (2002) Binding to cisplatin-modified DNA by the *Saccharomyces cerevisiae* HMGB protein Nhp6A, *Biochemistry 41*, 5404−5414.
36. Pöhler, J. R., Norman, D. G., Bramham, J., Bianchi, M. E., and Lilley, D. M. J. (1998) HMG box proteins bind to four-way DNA junctions in their open conformation, *EMBO J. 17*, 817−826.
37. Chow, C. S., Whitehead, J. P., and Lippard, S. J. (1994) HMG domain proteins induce sharp bends in cisplatin-modified DNA, *Biochemistry 33*, 15124−15130.
38. He, Q., Ohndorf, U. M., and Lippard, S. J. (2000) Intercalating residues determine the mode of HMG1 domains A and B binding to cisplatin-modified DNA, *Biochemistry 39*, 14426−14435.
39. Jung, Y., and Lippard S. J. (2003) Nature of full-length HMGB1 binding to cisplatin-modified DNA, *Biochemistry 42*, 2664−2671.

BI0522798